Supporting Information for

Defect-rich $W_{1-x}Mo_xS_2$ solution for efficient H_2 evolution in acidic electrolyte

Zongge Li[a,*], Zhicheng Liu[b], Danni Wang[b], Wenjun Kang[a], Haibo Li[a] and Guoxin Zhang[b,*]

a. Shandong Provincial Key Laboratory of Chemical Energy Storage and Novel Cell Technology, School of Chemistry and Chemical Engineering, Liaocheng University, Liaocheng 252059, China. Email: lizongge@lcu.edu.cn

b. College of Energy Storage Technology, Shandong University of Science and Technology, Qingdao, Shandong 266590, China. E-mail: zhanggx@sdust.edu.cn

1. Experimental Section

1.1 Chemicals. Molybdenum (V) chloride ($MoCl_5$, A.R. grade) and tungsten hexachloride (WCl_6, A.R. grade) were bought from Shanghai Macklin Biochemical Co., Ltd. Formamide (CH_3NO, purity>99%) was brought from Tianjin Damao Chemical Factory. Sulfur powder and absolute ethanol were purchased from Sinopharm Chemical Reagent Co. Ltd. Nafion solution (5.0 wt.%, Dupont) and commercial Pt/C (20.0 wt.%) were bought from Shanghai Hesen Electric Co., Ltd. Carbon black (BP2000) was purchased from Nanjing Xianfeng Nanomaterial Technology Co., Ltd. Carbon paper (Toray Industries). All reagents were used as received without further purification.

1.2 Preparation of $W_{0.4}Mo_{0.6}S_2$ materials

The $W_{0.4}Mo_{0.6}S_2$ was prepared via a stepwise method consisting of solvothermal treatment of W^{6+}/Mo^{5+}/formamide solution and subsequent inert annealing of f-$W_{0.4}Mo_{0.6}$-NC precursor in S vapor. Typically, 0.60 mmol MoCl5 and 0.40 mmol WCl_6 (in a W to Mo mole ratio of 2:3) were dissolved in 30.0 mL formamide under sonication of 30 min to form a homogeneous solution. Then, the solution was transferred into a 50.0 mL Teflon-lined stainless-steel autoclave, maintained at 180 ℃ for 12 h, and allowed to cool to room temperature naturally. The slurry product was washed with water and absolute ethanol 2-3 times and dried at 60℃ overnight. Next, 0.10 g of the obtained precursor was placed at the center of a quartz tube furnace. Sulfur powder (1.0 g) was placed in the upstream region of the quartz tube 10 cm away from the precursor. After being flushed with N_2 for 30 min, the tube furnace was heated from room temperature to 600 ℃ at a rate of 5 ℃ min^{-1} and maintained for 1 h. The obtained sample was named $MoWS_x$. To prepare more $W_{1-x}Mo_xS_2$, different mole ratios of Mo and W with a total mole of 1 mmol were used.

1.3. Materials characterizations

Powder X-ray diffraction (XRD) was performed using a Bruker D8 Advance

diffractometer at 40 kV and 40 mA using Cu Ka radiation (λ = 0.15406 nm). Scanning electron microscopy (SEM) was performed using an Apreo S HiVac scanning electron microscope at an acceleration voltage of 15 kV. Transmission electron microscopy (TEM), high-resolution TEM (HRTEM) images, and EDS mapping images were obtained using a FEI Talos 200S high-resolution transmission electron microscope at an acceleration voltage of 200 kV. Raman spectra were obtained using a DXR2 Raman Microscope (Thermo Fisher) with a 532 nm line of Ar laser as the excitation source. X-ray photoelectron spectrum (XPS) analysis was performed using a PHI 5000 Versaprobe system using monochromatic Al Ka radiation (1486.6 eV). All binding energies were referenced to the C1s peak at 284.6 eV.

1.4. Electrochemical measurements

All the electrochemical measurements were performed on a typical three-electrode system using a CHI 760e electrochemical station (Shanghai Chenhua Co.) at room temperature. In this system, the as-prepared catalysts, a graphite rod, and saturated calomel electrode (SCE) were used as the working electrode, counter electrode, and reference electrode, respectively. For comparison, the commercial Pt/C and RuO_2 were dispersed by ultrasonic treatment and then pipetted onto the Carbon paper for electrochemical test. Before data collection, all working electrodes were pretreated by cyclic voltammetry (CV) scanning at 100 mV s^{-1} in the same electrolyte used for HER measurement to fully activate the accessible surface of electrode materials. Linear sweep voltammetry (LSV) polarization curves were obtained with a scan rate of 5.0 mV s^{-1} in 0.5 M H_2SO_4 solution. To compare our work with other literature, all the current densities in this work were normalized by electrode geometric area. All the potentials were converted to the potential versus the reversible hydrogen electrode (RHE) according to E(RHE)=E(SCE)+0.241 V+0.059 V×pH. LSV curves were obtained without *i*R-compensation at a scan rate of 5 mV s^{-1}. The electrochemical impedance spectroscopy (EIS) measurements were tested in 0.5 M H_2SO_4 solution at open-circuit voltage with a frequency from 10 mHz to 100 kHz at an amplitude of 5.0

mV. A long-term stability test was recorded by taking a chronoamperometric curve at a constant overpotential.

For electrochemical surface area (ECSA) normalized current density, ESCA was estimated by measuring the electrical double-layer capacitance (C_{dl}). For the evaluation of electrochemical double-layer capacitance (C_{dl}), cyclic voltammograms (CV) were recorded at different scan rates (20-100 mV s^{-1}). The electrochemically active surface area (ECSA) was calculated from C_{dl} value using the relation,

$$ECSA = \frac{C_{dl}}{Cs} \tag{1}$$

where Cs is the specific capacitance of the electrode with a smooth planar surface. Cs of 0.040 mF cm^{-2} were used according to the reported literature. Then, the current densities of the samples were normalized by ECSA value according to the equation.

$$J_{ECSA} = \frac{J}{ECSA} \tag{2}$$

where J is the current density based on the geometrical surface area of the electrode (1 cm^2). The turnover frequency (TOF) is the number of transformations for a single active site per unit of time. The value of TOF can be calculated according to the following formula:

We calculated the number of active sites (n, mol) by testing the cyclic voltammetry curve of the sample in phosphoric acid buffer solution (PBS solution) with pH=7 (potential range −0.2 ~ 0.6 V vs. RHE, sweep speed 50 mV·s^{-1}). When no specific REDOX peak is observed in this interval, and assuming that the entire oxidation and reduction processes are single-electron processes, then the total number of active sites should be proportional to the charge in the entire potential interval, so that the maximum active site can be obtained from formula (3).

$$n = \frac{Q}{2F} = \frac{i \times t}{2F} = \frac{i \times V/\mu}{2F} = \frac{S}{2F \times \mu}$$

(3)

$$TOF = \frac{|J|A}{mFn} \quad (4)$$

where n is the number of active sites, S represents the effective area obtained by the cyclic voltammetry curve integral, and μ represents the sweep speed. F is the faradaic constant, m is the number of electrons consumed to form an H_2 molecule, J is the absolute value of the current density in the polarization curve (LSV), and A is the area of the electrode under measurement.

The principle of the EIS fitting circuit is as follows, where Rs is solution resistance, Rct is charge transfer resistance and CPE is the double-layer capacitance. The charge transfer resistance (Rct) of all electrodes was determined from the EIS. Circuit fits very well with all the samples.

2. Supplementary figures

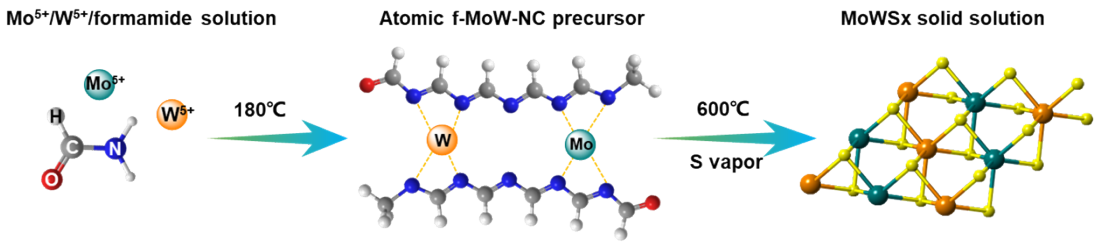

Figure S1. Graphical scheme for the synthesis of defect-rich $WMoS_2$ solid solution

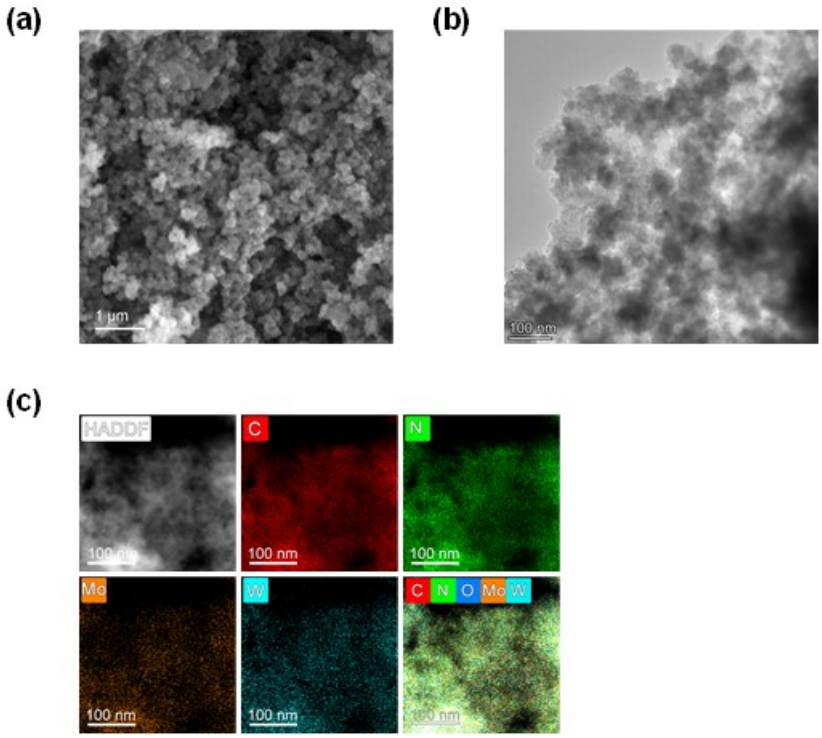

Figure S2. (**a**) SEM image, (**b**) TEM image, and (**c**) HRTEM-HAADF image and element mapping images of $W_{0.4}Mo_{0.6}$-NC-180 precursor.

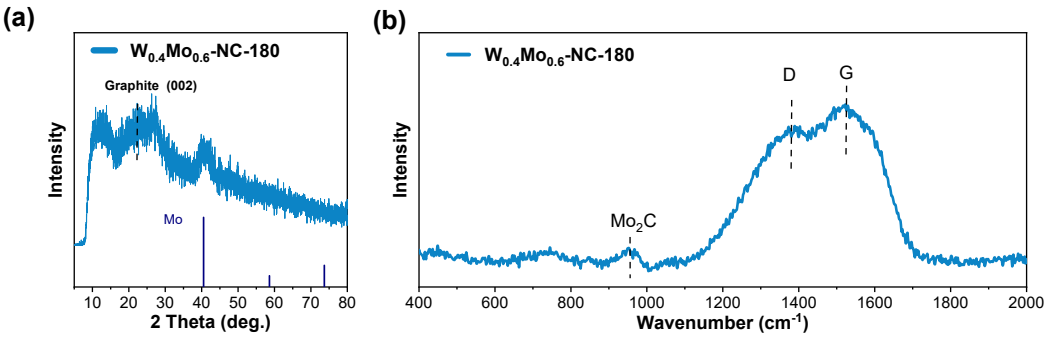

Figure S3. (**a**) XRD patterns and (**b**) Raman spectra of $W_{0.4}Mo_{0.6}$-NC precursor.

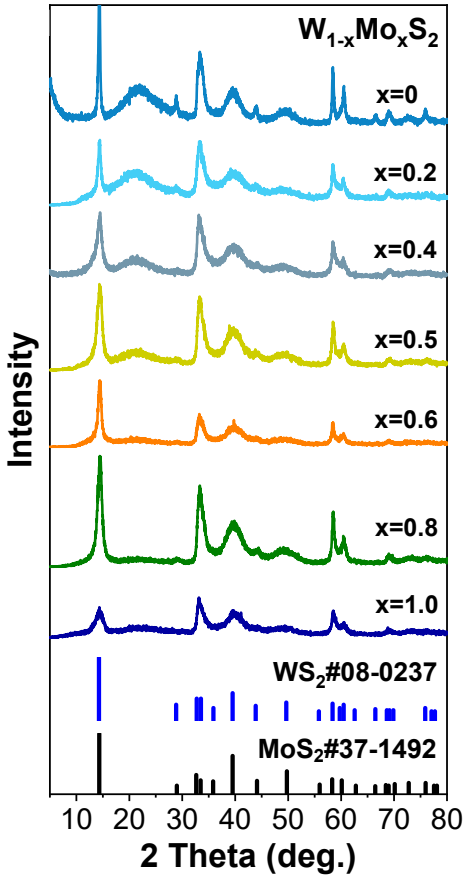

Figure S4. XRD patterns of $W_{1-x}Mo_xS_2$

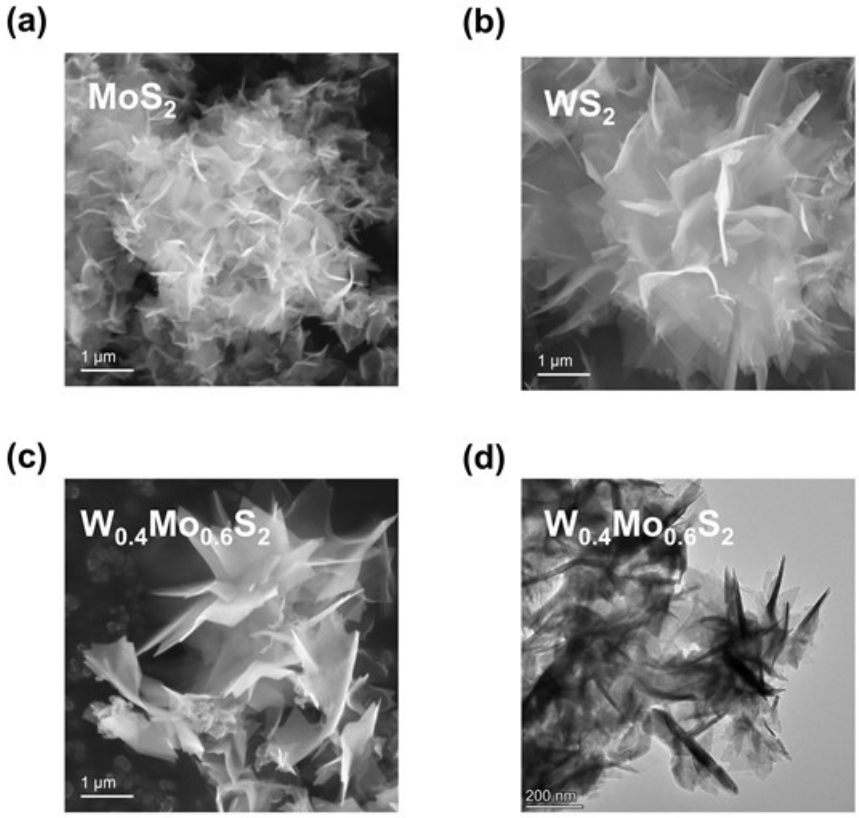

Figure 5. (**a**) SEM image of MoS_2, (**b**) SEM image of WS_2, (**c**) SEM image of $W_{0.4}Mo_{0.6}S_2$. (**d**) TEM image of $W_{0.4}Mo_{0.6}S_2$.

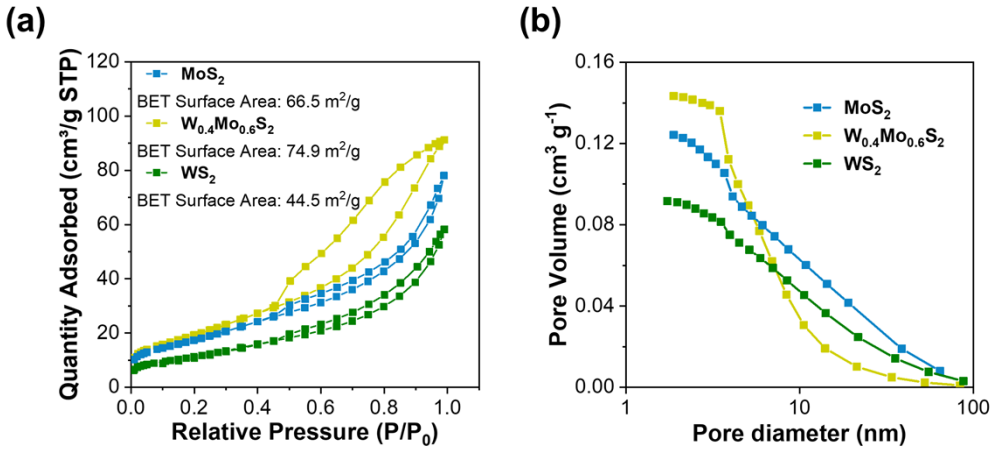

Figure S6. (**a**) N_2 adsorption/desorption isotherm and (**b**) pore distribution curves of WS_2, $W_{0.4}Mo_{0.6}S_2$ and MoS_2.

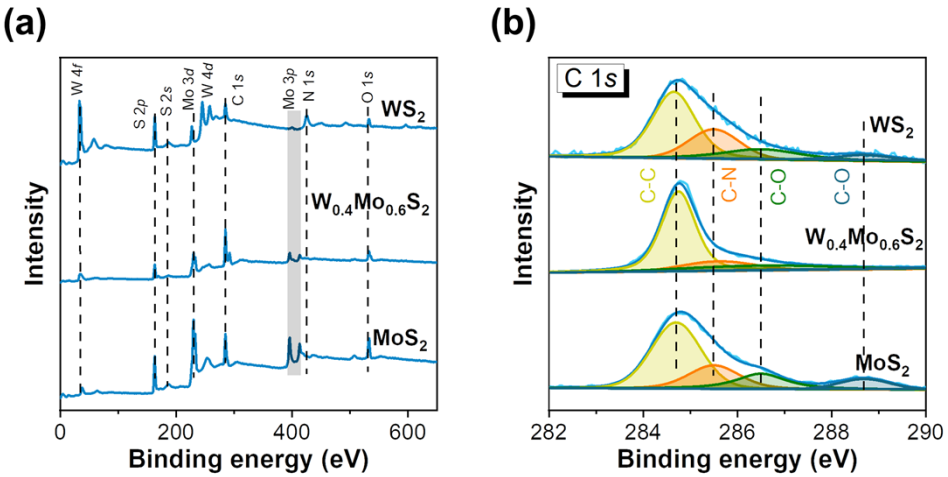

Figure S7. (**a**) XPS survey spectra and (**b**) C *1s* spectra of WS_2, $W_{0.4}Mo_{0.6}S_2$ and MoS_2.

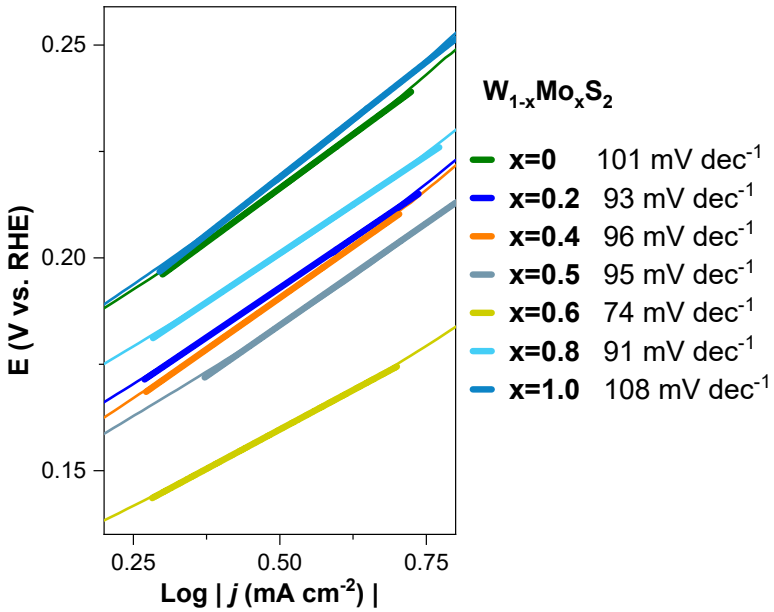

Figure S8. Tafel plots of samples in 0.5 M H_2SO_4.

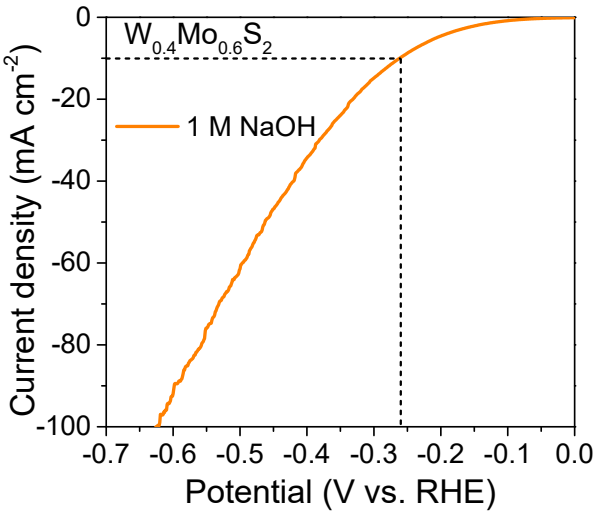

Figure S9. The HER polarization curves of $W_{0.4}Mo_{0.6}S_2$ in 1M NaOH solution

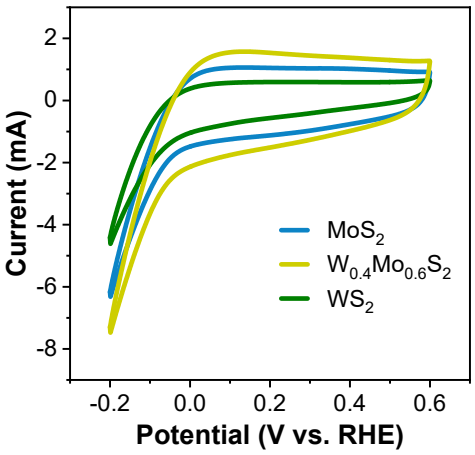

Figure S10. CVs of the hybrid catalysts at pH = 7 PBS with a scan rate of 50 mV·s^{-1}

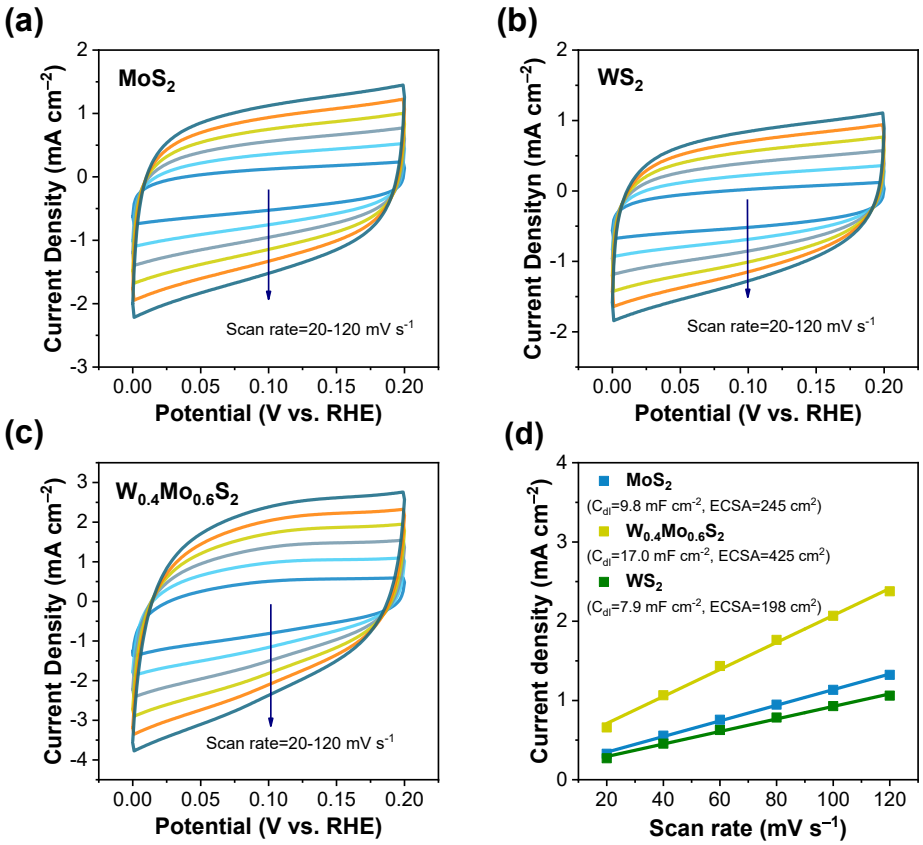

Figure S11. Cyclic voltammograms of (**a**) MoS_2, (**b**) WS_2, and (**c**) $W_{0.4}Mo_{0.6}S_2$ at different rates ranging from 20−120 mV s^{-1} in the potential region from 0−0.2 V. (**d**) plots of the capacitive currents as a function of scan rate, with electrochemical double-layer capacitance (C_{dl}), and electrochemical surface area (ECSA) marked in figures.

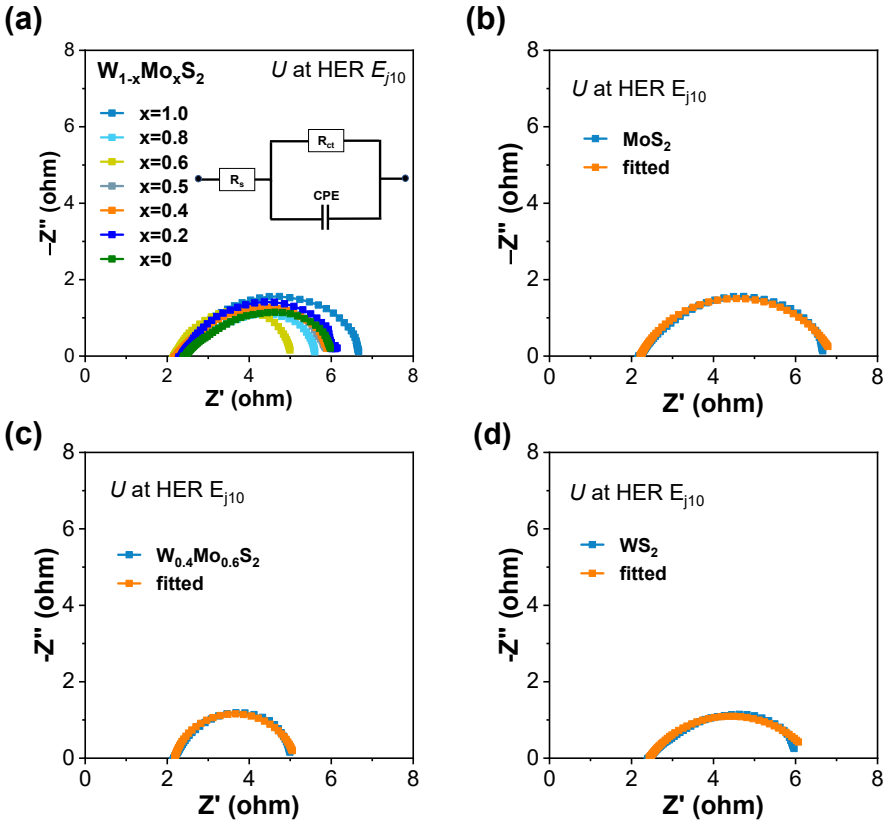

Figure S12. (**a**) EIS curves. (**b-d**) Electrochemical impedance circuit fitting of (**b**) MoS_2, (**c**) WS_2, and (**d**) $W_{0.4}Mo_{0.6}S_2$.

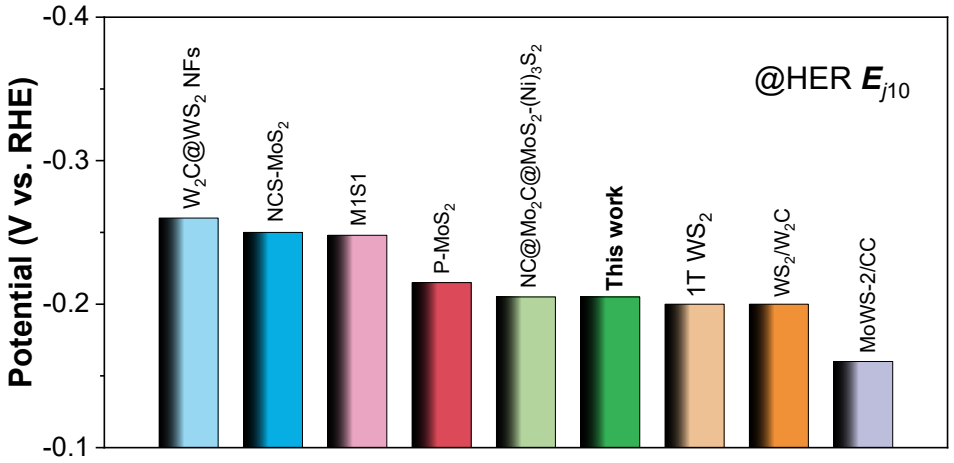

Figure S13. In comparison to HER performance in acidic media, the HER electrochemical performance of the $W_{0.4}Mo_{0.6}S_2$ is superior to or at least parallel to previously reported sulfides[1-10].

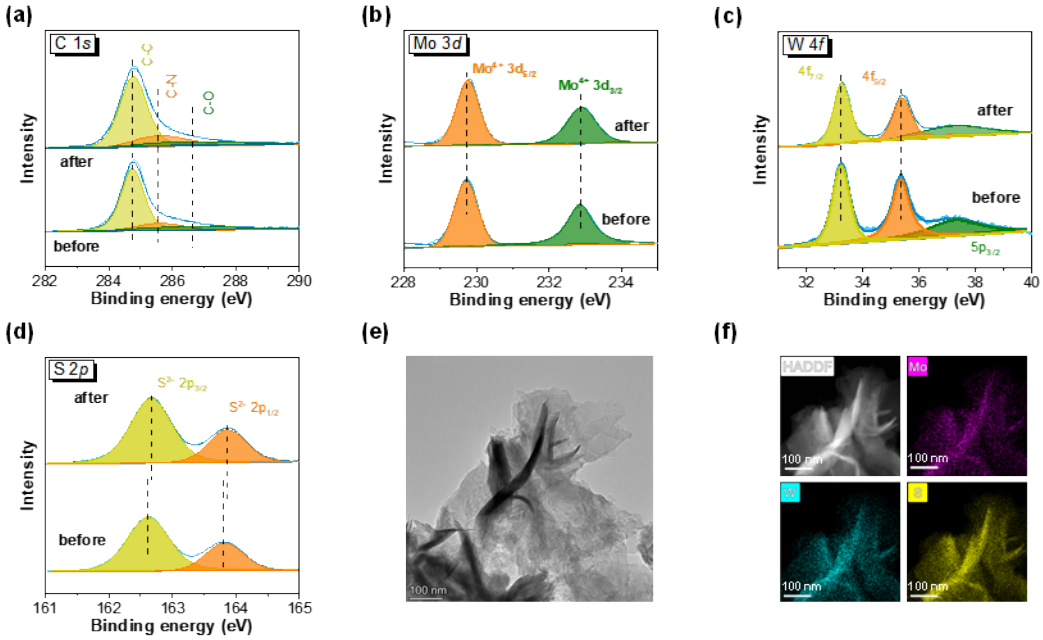

Figure S14. XPS analysis of $W_{0.4}Mo_{0.6}S_2$ before and after Long-term stability test in 0.5M H_2SO_4: (**a**) C 1*s*, (**b**) Mo 3*d*, (**c**) W 4*f*, (**d**) S 2*p* spectra. (**e**) TEM image and (**f**) HRTEM-HAADF image and element mapping images of $W_{0.4}Mo_{0.6}S_2$ after long-term stability test.

Table S1. Element contents of WS_2, $W_{0.4}Mo_{0.6}S_2$, and MoS_2 measured by XPS.

Sample	C (at.%)	O (at.%)	N (at.%)	W (at.%)	Mo (at.%)	S (at.%)
MoS_2	51.52	15.38	1.28	-	10.46	21.36
$Mo_{0.6}W_{0.4}S_2$	71.89	9.45	1.28	1.67	4.79	10.93
WS_2	38.86	8.71	4.02	14.84	-	33.57

Table S2. EIS circuit fitting parameters of different catalysts.

Circuit component	**MoS_2**	**$Mo_{0.6}W_{0.4}S_2$**	**WS_2**
R_s/Ω	2.274	2.183	2.434
R_{ct}/Ω	4.709	2.929	3.977
CPE/F	0.008	0.026	0.021

Table S3. Element contents of $W_{0.4}Mo_{0.6}S_2$ before and after long-term stability test measured by XPS.

Sample	C (at.%)	O (at.%)	N (at.%)	W (at.%)	Mo (at.%)	S (at.%)
before	71.89	9.45	1.28	1.67	4.79	10.93
after	69.55	7.13	1.34	2.06	5.59	14.32

References

1. T. Liang, H. Jia, Y. Zhou, J. Fan, Y. Xu, Y. Hu, L. Zhou, C. Wang, F. Chen, P. Guan, M. Li, T. Wan, M. Ferry and D. Chu, *New Journal of Chemistry*, 2022, **46**, 23344-23350.
2. Q. Xu, Y. Zhang, Y. Zheng, Y. Liu, Z. Tian, Y. Shi, Z. Wang, J. Ma and W. Zheng, *The Journal of Physical Chemistry C*, 2021, **125**, 11369-11379.
3. J.-T. Ren, Y.-J. Song and Z.-Y. Yuan, *Journal of Energy Chemistry*, 2019, **32**, 78-84.
4. J. Wang, N. Wang, Y. Guo, J. Yang, J. Wang, F. Wang, J. Sun, H. Xu, Z.-H. Liu and R. Jiang, *ACS Sustainable Chemistry & Engineering*, 2018, **6**, 13435-13442.
5. Z. Liu, N. Li, C. Su, H. Zhao, L. Xu, Z. Yin, J. Li and Y. Du, *Nano Energy*, 2018, **50**, 176-181.
6. L. Gong, X. Mu, Q. Li, L. Ma, Y. Xiong and R. Li, *International Journal of Hydrogen Energy*, 2021, **46**, 5250-5258.
7. T. P. Nguyen, S. Y. Kim, T. H. Lee, H. W. Jang, Q. V. Le and I. T. Kim, *Applied Surface Science*, 2020, **504**, 144389.
8. X. Ren, F. Yang, R. Chen, P. Ren and Y. Wang, *New Journal of Chemistry*, 2020, **44**, 1493-1499.
9. B. Chen, P. Hu, F. Yang, X. Hua, F. F. Yang, F. Zhu, R. Sun, K. Hao, K. Wang and Z. Yin, *Small*, 2023, **19**, e2207177.
10. H. Wang, Z. Xu, Z. Zhang, S. Hu, M. Ma, Z. Zhang, W. Zhou and H. Liu, *Nanoscale*, 2020, **12**, 22541-22550.